Nearly model-independent constraints on dense matter equation of state in a Bayesian approach

N. K. Patra[1] Sk Md Adil Imam[2,3] B. K. Agrawal[2,3,*] Arunava Mukherjee[2,3] and Tuhin Malik[4]

[1]*Department of Physics, BITS-Pilani, K. K. Birla Goa Campus, Goa 403726, India*
[2]*Saha Institute of Nuclear Physics, 1/AF Bidhannagar, Kolkata 700064, India*
[3]*Homi Bhabha National Institute, Anushakti Nagar, Mumbai 400094, India*
[4]*CFisUC, Department of Physics, University of Coimbra, 3004-516 Coimbra, Portugal*

We apply a Bayesian approach to construct a large number of minimally constrained equations of state (EOSs) and study their correlations with a few selected properties of a neutron star (NS). Our set of minimal constraints includes a few basic properties of saturated nuclear matter and low-density pure neutron matter EOS which is obtained from a precise next-to-next-to-next-to-leading-order (N^{3}LO) calculation in chiral effective field theory. The tidal deformability and radius of a NS with mass 1–2 $M_\odot$ are found to be strongly correlated with the pressure of β-equilibrated matter at densities higher than the saturation density ($\rho_0 = 0.16$ fm^{-3}) in a nearly model-independent manner. These correlations are employed to parametrize the pressure for β-equilibrated matter, around $2\rho_0$, as a function of neutron star mass and the corresponding tidal deformability. The maximum mass of the neutron star is also found to be strongly correlated with the pressure of β-equilibrated matter at densities $\sim 4.5\rho_0$.

I. INTRODUCTION

Gravitational-wave astronomy promises unprecedented constraints on the equation of state (EOS) of neutron star matter through the detailed properties of the gravitational waveform observed during the merging of binary neutron stars (BNSs). In addition, x-ray observations from the Neutron Star Interior Composition Explorer (NICER) instruments have also provided a compelling constraint on the equation of state independently. The tidal deformability parameters inferred from these gravitational-wave events encode information about the EOS. For the first time, a BNS event (GW170817) was observed by the LIGO-Virgo detector from a low-mass compact binary neutron star merger with a total mass of the system $2.74^{+0.04}_{-0.01}$ $M_\odot$ [1,2]. Another gravitational-wave event likely originating from the coalescence of BNSs, GW190425, was observed [3] subsequently. These two events have already triggered many theoretical investigations to constrain the EOS of neutron star matter [3–12]. The upcoming runs of LIGO-Virgo-KAGRA and the future detectors, e.g., Einstein Telescope (ET) and Cosmic Explorer (CE), are expected to observe many more BNS signals emitted from coalescing neutron stars. The mass and radius of NSs, observed either in isolation or in binaries, by NICER [13–15] have offered complementary constraints on the EOS. A sufficiently large number of such observations over a wide range of NS masses may be employed to constrain several key quantities associated with the EOS of β-equilibrated matter which are not readily accessible in the terrestrial laboratory. The behavior of the EOS at suprasaturation densities is generally studied using the observed maximum neutron star mass, together with radius and tidal deformability corresponding to the neutron star with canonical mass 1.4 $M_\odot$ [16–18]. Recently, in Refs. [19–24], efforts were made to constrain the EOS of β-equilibrated matter which is relevant to the studies of NS properties. The values of tidal deformability of NSs with mass 1–2 $M_\odot$ are found to be strongly correlated with the EOS at twice the saturation density.

Statistical tools are quite helpful in providing a quantitative interpretation of NS observables. A Bayesian approach is often applied to analyze gravitational-wave signals, which involves nearly 15 parameters for binary compact object mergers, to infer their source properties [25]. It has been also extended to investigate the properties of short gamma-ray bursts [26], neutron stars [27–29], the formation history of binary compact objects [30–34], and to test general relativity [35–38]. Of late, the Bayesian approach has become a useful statistical tool for parameter estimation in the field of nuclear physics and nuclear astrophysics [39]. It allows one to obtain joint posterior distributions of the model parameters and the correlations among them for a given set of data. Various constraints on the parameters known *a priori* are incorporated through their prior distributions. Bayesian techniques have also

*bijay.agrawal@saha.ac.in

been employed to constrain symmetry energy [40], masses, and radii of NSs [41] using the bounds on the EOS obtained from chiral effective field theory. Bayesian techniques have been extensively applied to constrain the EOS for symmetric nuclear matter, β-equilibrated matter (BEM), and density dependence of symmetry energy coefficient using various finite nuclei and NS properties [42–53].

We use a Bayesian approach to construct large sets of EOSs which correspond to the Taylor and $\frac{n}{3}$ expansions [53]. The expansion coefficients in the former case are the individual nuclear matter parameters (NMPs), whereas in the latter case they are their linear combinations. The EOSs are consistent with a set of minimal constraints that includes a few low-order nuclear matter parameters at the saturation density and the EOS for the pure neutron matter (PNM) at low densities obtained from a precise next-to-next-to-next-to-leading-order (N³LO) calculation in chiral effective field theory. The marginalized posterior distributions of NMPs and the various NS properties obtained from the set of minimal constraints are found to be within reasonable bounds. The correlations of various NS properties, such as tidal deformability, radius, and maximum mass, with key EOS parameters are studied. These correlations are investigated for a wide range of NS masses and densities for the EOS.

The paper is organized as follows. The Taylor and $\frac{n}{3}$ expansions for the EOS of neutron star matter and the Bayesian approach are briefly outlined in Sec. II. The results for the posterior distributions of nuclear matter parameters and associated NS properties together with their correlations with some key quantities associated with EOSs are presented in Sec. III. The main outcomes of the present investigation are summarized in Sec. IV.

II. METHODOLOGY

The energy per nucleon for neutron star matter $E(\rho, \delta)$ at a given total nucleon density ρ and asymmetry δ can be decomposed into the energy per nucleon for the symmetric nuclear matter, $E(\rho, 0)$, and the density-dependent symmetry energy $E_{\text{sym}}(\rho)$ in the parabolic approximation as

$$E(\rho, \delta) = E(\rho, 0) + E_{\text{sym}}(\rho)\delta^2 + \cdots, \qquad (1)$$

where $\delta = \left(\frac{\rho_n - \rho_p}{\rho}\right)$ with ρ_n and ρ_p being the neutron and proton densities, respectively. The value of δ at a given ρ is determined by the condition of β equilibrium and the charge neutrality. Once δ is known, the fraction of neutrons, protons, electrons, and muons can be easily evaluated. In the following, we expand $E(\rho, 0)$ and $E_{\text{sym}}(\rho)$ appearing in Eq. (1) using Taylor and $\frac{n}{3}$ expansions. The coefficients of expansion in the case of Taylor correspond to the individual nuclear matter parameters. In the latter case, they are expressed as linear combinations of the nuclear matter parameters.

A. Taylor's expansion

The $E(\rho, 0)$ and $E_{\text{sym}}(\rho)$ can be expanded around the saturation density ρ_0 as [54–58]

$$E(\rho, 0) = \sum_n \frac{a_n}{n!}\left(\frac{\rho - \rho_0}{3\rho_0}\right)^n, \qquad (2)$$

$$E_{\text{sym}}(\rho) = \sum_n \frac{b_n}{n!}\left(\frac{\rho - \rho_0}{3\rho_0}\right)^n, \qquad (3)$$

so that

$$E(\rho, \delta) = \sum_n \frac{1}{n!}(a_n + b_n\delta^2)\left(\frac{\rho - \rho_0}{3\rho_0}\right)^n, \qquad (4)$$

where the coefficients a_n and b_n are the nuclear matter parameters. We truncate the sum in Eqs. (2) and (3) at fourth order; i.e., $n = 0$–4. Therefore, the coefficients a_n and b_n correspond, respectively, to

$$a_n \equiv \varepsilon_0, 0, K_0, Q_0, Z_0, \qquad (5)$$

$$b_n \equiv J_0, L_0, K_{\text{sym},0}, Q_{\text{sym},0}, Z_{\text{sym},0}. \qquad (6)$$

In Eqs. (5) and (6), ε_0 is the binding energy per nucleon, K_0 the incompressibility coefficient, J_0 the symmetry energy coefficient, L_0 its slope parameter, and $K_{\text{sym},0}$ the symmetry energy curvature parameter, and $Q_0(Q_{\text{sym},0})$ and $Z_0(Z_{\text{sym},0})$ are related to third- and fourth-order density derivatives of $E(\rho, 0)$ [$E_{\text{sym}}(\rho)$], respectively. The subscript zero indicates that all the nuclear matter parameters are calculated at the saturation density.

It may be noticed from Eq. (4) that the coefficients a_n and b_n may display some correlations among themselves provided the asymmetry parameter depends weakly on the density. Furthermore, Eq. (4) may converge slowly at high densities, i.e., $\rho \gg 4\rho_0$. This situation is encountered for the heavier neutron stars. Neutron stars with a mass around $2\,M_\odot$ typically have central densities $\sim$4–6ρ_0.

B. $\frac{n}{3}$ expansion

An alternative expansion of $E(\rho, \delta)$ can be obtained by expanding $E(\rho, 0)$ and $E_{\text{sym}}(\rho)$ as [59,60]

$$E(\rho, 0) = \sum_{n=2}^{6}(a'_{n-2})\left(\frac{\rho}{\rho_0}\right)^{\frac{n}{3}}, \qquad (7)$$

$$E_{\text{sym}}(\rho) = \sum_{n=2}^{6}(b'_{n-2})\left(\frac{\rho}{\rho_0}\right)^{\frac{n}{3}}, \qquad (8)$$

$$E(\rho, \delta) = \sum_{n=2}^{6}(a'_{n-2} + b'_{n-2}\delta^2)\left(\frac{\rho}{\rho_0}\right)^{\frac{n}{3}}. \qquad (9)$$

We refer to this as the $\frac{n}{3}$ expansion. It is now evident from Eqs. (7) and (8) that the coefficients of expansion are no longer the individual nuclear matter parameters, unlike in the case of Taylor's expansion. The values of the nuclear matter parameters can be expressed in terms of the expansion coefficients a' and b' as, respectively,

$$
\begin{pmatrix} \varepsilon_0 \\ 0 \\ K_0 \\ Q_0 \\ Z_0 \end{pmatrix} = \begin{pmatrix} 1 & 1 & 1 & 1 & 1 \\ 2 & 3 & 4 & 5 & 6 \\ -2 & 0 & 4 & 10 & 18 \\ 8 & 0 & -8 & -10 & 0 \\ -56 & 0 & 40 & 40 & 0 \end{pmatrix} \begin{pmatrix} a'_0 \\ a'_1 \\ a'_2 \\ a'_3 \\ a'_4 \end{pmatrix}, \qquad (10)
$$

$$
\begin{pmatrix} J_0 \\ L_0 \\ K_{\text{sym},0} \\ Q_{\text{sym},0} \\ Z_{\text{sym},0} \end{pmatrix} = \begin{pmatrix} 1 & 1 & 1 & 1 & 1 \\ 2 & 3 & 4 & 5 & 6 \\ -2 & 0 & 4 & 10 & 18 \\ 8 & 0 & -8 & -10 & 0 \\ -56 & 0 & 40 & 40 & 0 \end{pmatrix} \begin{pmatrix} b'_0 \\ b'_1 \\ b'_2 \\ b'_3 \\ b'_4 \end{pmatrix}. \qquad (11)
$$

The relations between the expansion coefficients and the nuclear matter parameters are governed by the nature of the functional form for $E(\rho,0)$ and $E_{\text{sym}}(\rho)$. The off-diagonal elements in the above matrices would vanish for the Taylor expansion of $E(\rho,0)$ and $E_{\text{sym}}(\rho)$ as given by Eqs. (2) and (3), respectively. Therefore, each of the expansion coefficients is simply the individual nuclear matter parameter given by Eqs. (5) and (6). Inverting the matrices in Eqs. (10) and (11), we have

$$
a'_0 = \frac{1}{24}(360\varepsilon_0 + 20K_0 + Z_0),
$$

$$
a'_1 = \frac{1}{24}(-960\varepsilon_0 - 56K_0 - 4Q_0 - 4Z_0),
$$

$$
a'_2 = \frac{1}{24}(1080\varepsilon_0 + 60K_0 + 12Q_0 + 6Z_0),
$$

$$
a'_3 = \frac{1}{24}(-576\varepsilon_0 - 32K_0 - 12Q_0 - 4Z_0),
$$

$$
a'_4 = \frac{1}{24}(120\varepsilon_0 + 8K_0 + 4Q_0 + Z_0), \qquad (12)
$$

$$
b'_0 = \frac{1}{24}(360J_0 - 120L_0 + 20K_{\text{sym},0} + Z_{\text{sym},0}),
$$

$$
b'_1 = \frac{1}{24}(-960J_0 + 328L_0 - 56K_{\text{sym},0} - 4Q_{\text{sym},0} - 4Z_{\text{sym},0}),
$$

$$
b'_2 = \frac{1}{24}(1080J_0 - 360L_0 + 60K_{\text{sym},0} + 12Q_{\text{sym},0} + 6Z_{\text{sym},0}),
$$

$$
b'_3 = \frac{1}{24}(-576J_0 + 192L_0 - 32K_{\text{sym},0} - 12Q_{\text{sym},0} - 4Z_{\text{sym},0}),
$$

$$
b'_4 = \frac{1}{24}(120J_0 - 40L_0 + 8K_{\text{sym},0} + 4Q_{\text{sym},0} + Z_{\text{sym},0}). \qquad (13)
$$

Each of the coefficients a' and b' is the linear combination of nuclear matter parameters in such a way that the lower-order parameters may contribute dominantly at low densities. The effects of higher-order parameters become prominent with the increase in density.

C. Bayesian estimation of nuclear matter parameters

A Bayesian approach enables one to carry out detailed statistical analysis of the parameters of a model for a given set of fit data. It yields joint posterior distributions of model parameters which can be used not only to study the distributions of given parameters but also to examine correlations among model parameters. One can also incorporate prior knowledge of the model parameters and various constraints on them through the prior distributions. This approach is mainly based on the Bayes theorem, which states that [61]

$$
P(\boldsymbol{\theta}|D) = \frac{\mathcal{L}(D|\boldsymbol{\theta})P(\boldsymbol{\theta})}{\mathcal{Z}}, \qquad (14)
$$

where $\boldsymbol{\theta}$ and D denote the set of model parameters and the fit data, respectively. The $P(\boldsymbol{\theta}|D)$ is the joint posterior distribution of the parameters, $\mathcal{L}(D|\boldsymbol{\theta})$ is the likelihood function, $P(\boldsymbol{\theta})$ is the prior for the model parameters, and $\mathcal{Z}$ is the evidence. The posterior distribution of a given parameter can be obtained by marginalizing $P(\boldsymbol{\theta}|D)$ over remaining parameters. The marginalized posterior distribution for a parameter θ_i can be obtained as

$$
P(\theta_i|D) = \int P(\boldsymbol{\theta}|D)\prod_{k \neq i} d\theta_k. \qquad (15)
$$

We use a Gaussian likelihood function defined as

$$
\mathcal{L}(D|\boldsymbol{\theta}) = \prod_j \frac{1}{\sqrt{2\pi\sigma_j^2}} e^{-\frac{1}{2}\left(\frac{d_j - m_j(\theta)}{\sigma_j}\right)^2}. \qquad (16)
$$

Here, the index j runs over all the data, and d_j and m_j are the data and corresponding model values, respectively. The σ_j are the adopted uncertainties. The evidence $\mathcal{Z}$ in Eq. (14) is obtained by complete marginalization of the likelihood function. It is relevant when employed to compare different models. However, in the present work, $\mathcal{Z}$ is not very relevant. To populate the posterior distribution of Eq. (14), we implement a nested sampling algorithm by invoking the Pymultinest nested sampling [62] in the Bayesian Inference Library [25].

III. RESULTS AND DISCUSSIONS

We obtained the EOSs for BEM using Taylor and $\frac{n}{3}$ expansions as discussed in previous Eqs. (4) and (9). The coefficients of the Taylor expansion are the individual

nuclear matter parameters, whereas they correspond to linear combinations of nuclear matter parameters for the $\frac{n}{3}$ expansion. We have constructed marginalized posterior distributions for the nuclear matter parameters by applying a Bayesian approach to both the expansions considered. The nuclear matter parameters or the corresponding EOSs are consistent with a set of minimal constraints that includes basic properties of saturated nuclear matter and low-density ($\rho = 0.08$–0.16 fm^{-3}) EOS for pure neutron matter from the (N^{3}LO) calculation in chiral effective field theory [63]. This large number of EOSs is employed to evaluate the properties of the neutron star such as tidal deformability, radius, and maximum mass. The correlations of neutron star properties with the pressure of β-equilibrated matter at a given density are studied. Most of these correlations are sensitive to the choice of the neutron star mass and EOS at a given density. Our results for the correlations of tidal deformability with pressure for β-equilibrated matter are analogous to those obtained using a diverse set of nonrelativistic and relativistic mean-field models (MFMs) that reemphasize their model independence. Such model-independent trends inspire us to parametrize the pressure for β-equilibrated matter around $2\rho_0$ in terms of neutron star mass and the corresponding tidal deformability.

A. Priors, likelihood, and filters

We apply a Bayesian approach to obtain two large sets of EOSs corresponding to the Taylor and $\frac{n}{3}$ expansions. The posterior distributions for the NMPs are obtained by subjecting the EOSs to a set of minimal constraints which include some basic properties of nuclear matter evaluated at the saturation density ρ_0 and EOS for the pure neutron matter at low density. The constraints on the nuclear matter parameters are incorporated through the priors and those from the EOS for the pure neutron matter through the likelihood function. Not all the nuclear matter parameters are well constrained. Only a very few low-order nuclear matter parameters constrained within narrow bounds are the binding energy per nucleon $\varepsilon_0 = -16.0 \pm 0.3$ MeV, nuclear matter incompressibility coefficients $K_0 = 240 \pm 50$ MeV for the symmetric nuclear matter, and symmetry energy coefficient $J_0 = 32.0 \pm 5$ MeV. The values of ε_0 and J_0 are very well constrained by the binding energy of finite nuclei over a wide range of nuclear masses [10,64–68]. The value of K_0 is constrained from the experimental data on the centroid energy of isoscalar giant monopole resonance in a few heavy nuclei [69,70]. The values of L_0 have been extracted from experimental data on a variety of phenomena in the finite nuclei as well as from neutron star observations. The model-independent estimate of L_0 is expected to be derived from the measurement of neutron-skin thickness in asymmetric nuclei. Recent measurement of neutron-skin thickness in ^{208}Pb nucleus yields $L_0 = 106 \pm 37$ MeV [71]. However, this value of L_0 has

only marginal overlap at the lower side with those determined using experimental data on isovector giant dipole resonances in several nuclei [72] and recent neutron star observations [73]. The remaining nuclear matter parameters Q_0, Z_0, $K_{\mathrm{sym},0}$, $Q_{\mathrm{sym},0}$, and $Z_{\mathrm{sym},0}$ are constrained only poorly [24,74–77]. The priors for the nuclear matter parameters employed in the present work are listed in Table I. The prior distributions of ε_0, K_0, and J_0 are assumed to be Gaussian with rather smaller width, whereas the other higher-order nuclear matter parameters correspond to Gaussian distribution with very large width. We have also repeated our calculations with uniform priors for the higher-order nuclear matter parameters, and the results for the median values are found to be practically unaltered and uncertainties are modified marginally, up to 10% (not shown). In what follows, we present only those results which are obtained with priors as listed in Table I.

We know that the direct application of the lattice QCD simulations is challenging to hadronic physics at finite density due to the sign problem in Monte Carlo simulations. However, analytical calculations in terms of the effective degrees of freedom at low energy ($\rho < \rho_0$) like chiral effective theory are valid with negligible uncertainty. The precise N^{3}LO calculations are usually fitted to the nucleon-deuteron scattering cross section or few-body observables and even saturation properties of heavier nuclei [78]. The low-density EOS for the pure neutron matter obtained from a (N^{3}LO) calculation in chiral effective field theory [63] is employed as pseudodata to obtain a simple likelihood function as given by Eq. (16). The d's and the σ's in Eq. (16) are the pseudodata for the energy per neutron and the corresponding uncertainties taken from Ref. [63], respectively. This has been employed in many of the past

TABLE I. The prior distributions of the nuclear matter parameters. The nuclear matter parameters considered are the binding energy per nucleon (ε_0), incompressibility coefficient (K_0), symmetry energy coefficient (J_0), its slope parameter (L_0), and symmetry energy curvature parameter ($K_{\mathrm{sym},0}$), and $Q_0(Q_{\mathrm{sym},0})$ and $Z_0(Z_{\mathrm{sym},0})$ are related to third- and fourth-order density derivatives of $E(\rho, 0)$ [$E_{\mathrm{sym}}(\rho)$], respectively. All the nuclear matter parameters are evaluated at saturation density $\rho_0 = 0.16$ fm^{-3}. The parameters of Gaussian distribution (G) are the mean (μ) and standard deviation (σ).

NMPs (in MeV)	Pr-Dist	μ	σ
ε_0	G	−16	0.3
K_0	G	240	50
Q_0	G	−400	400
Z_0	G	1500	1500
J_0	G	32	5
L_0	G	50	50
$K_{\mathrm{sym},0}$	G	−100	200
$Q_{\mathrm{sym},0}$	G	550	400
$Z_{\mathrm{sym},0}$	G	−2000	2000

analyses as their pseudodata [22,79–82]. We have considered the values of energy per neutron over the density range $\rho = 0.08$–0.16 fm^{-3}. At densities lower than 0.08 fm^{-3}, the neutron star matter is expected to be clusterized.

We have filtered the nuclear matter parameters by demanding that (i) the pressure for the β-equilibrated matter should increase monotonically with density (thermodynamic stability), (ii) the speed of sound must not exceed the speed of light (causality), and (iii) the maximum mass of the neutron star must exceed $2 M_\odot$ (observational constraint). The causality breaks down at higher density mostly for the Taylor EOS. In such cases, we use the stiffest EOS, $P(\epsilon) = P_m + (\epsilon - \epsilon_m)$, where P_m and ϵ_m are the pressure and corresponding energy density at which the causality breaks, respectively [83].

B. Posterior distribution of nuclear matter parameters

To undertake the correlation systematics as proposed, we need a large number of EOSs with diverse behavior and corresponding neutron star properties. The posterior distributions for the nuclear matter parameters for the Taylor and $\frac{n}{3}$ expansions are obtained by subjecting the EOS to a set of minimal constraints as discussed above. The joint posterior distribution of the NMPs for a given model depends on the product of the likelihood and the prior distribution of nuclear matter parameters [Eq. (14)]. The posterior distribution of each individual parameter is obtained by marginalizing the joint posterior distribution with the remaining model parameters. If the marginalized posterior distribution of a nuclear matter parameter is localized more than the corresponding prior distribution, then the nuclear matter parameter is said to be well constrained by the data used for model fitting.

The corner plots for the marginalized posterior distributions for the nuclear matter parameters in one and two dimensions obtained for Taylor and $\frac{n}{3}$ expansions are displayed in Figs. 1 and 2, respectively. The differences between the one-dimensional posterior distributions for the nuclear matter parameters and corresponding prior distributions reflect the role of low-density EOSs for pure neutron matter in constraining the nuclear matter parameters. The EOS for the pure neutron matter mainly constrains the values of J_0, L_0, and $K_{sym,0}$ and to some extent $Q_{sym,0}$ and $Z_{sym,0}$. The shapes and the orientations of the confidence ellipses suggest that the correlations among most of the NMPs are weak. Most strong correlations exist only between $Q_0 - Z_0$, $L_0 - J_0$, and $L_0 - K_{sym,0}$ for both the expansions with correlation coefficient r $\simeq 0.8$. The $K_0 - Q_0$ correlation is slightly better in the case of $\frac{n}{3}$ expansion (r ~ -0.6) as compared to Taylor (r ~ -0.18). The median values of the nuclear matter parameters and the corresponding 68% (90%) confidence intervals obtained from the marginalized posterior distributions are listed in Table III (see the Appendix). We also provide the values for the nuclear matter parameters obtained without the PNM

constraints. The low-density pure neutron matter mainly constrains those nuclear matter parameters which are associated with the density dependence of the symmetry energy. The median values of L_0 and $K_{sym,0}$, which determined the linear and quadratic density dependence of the symmetry energy, become smaller, suggesting softer symmetry energy "at high density" with the inclusion of pure neutron matter constraints. Furthermore, the uncertainties on L_0 reduced by more than 50%. The median value of $Q_{sym,0}$ remain more or less unaltered. From the recent measurement of the neutron-skin thickness for ^{208}Pb nucleus (PREX-II) [71,84], $\Delta R_{skin} = 0.283 \pm 0.071$ fm, the value of L_0 has been determined to be 106 ± 37 MeV [71]. This value of L_0 agrees with the ones obtained in the present work with PNM constrained only within 90% confidence interval.

C. Properties of neutron stars

Once the EOS for the core and crust are known, the values of NS mass, radius, and tidal deformability corresponding to a given central pressure can be obtained by solving Tolman-Oppenheimer-Volkoff equations [85,86]. The EOSs for the core region of a neutron star, correspond to the β-equilibrated matter over the density range 0.5–$8\rho_0$, are obtained from the posterior distributions of nuclear matter parameters for the Taylor and $\frac{n}{3}$ expansions. The core EOSs are matched to the crust EOSs for obtaining the NS properties. The EOS for the outer crust is taken to be the one given by Baym, Pethick, and Sutherland [87]. The inner crust that joins the inner edge of the outer crust and the outer edge of the core is assumed to be polytropic [88]: $p(\epsilon) = c_1 + c_2 \epsilon^\gamma$. Here, the parameters c_1 and c_2 are determined in such a way that the EOS for the inner crust matches with the outer crust at one end ($\rho = 10^{-4}$ fm^{-3}) and with the core at the other end ($0.5\rho_0$). The polytropic index γ is taken to be equal to $4/3$. The radii of neutron stars with mass $\sim 1 M_\odot$ are more sensitive to the treatment of crust EOSs [89]. It is demonstrated that the treatment of crust EOSs employed in the present work may introduce uncertainties of about 50–100 m in the radii of NSs having mass $1.4 M_\odot$. It is shown in Ref. [90] that the choice of EOS for the inner crust does not significantly impact the values of tidal deformability which depends on the Love number k_2 as well as the compactness parameter.

We have obtained the distributions of $\Lambda_{1.4}$, $R_{1.4}$, $R_{2.07}$, and M_{max} using the posterior distributions for the nuclear matter parameters corresponding to the Taylor and $\frac{n}{3}$ expansions. The corner plots for these NS properties are displayed in Fig. 3. The effective priors for the NS properties as shown by green lines are obtained using the priors for the nuclear matter parameters. The posterior distributions of NS properties are narrower than the corresponding effective priors, indicating the significance of the low-density EOS for the pure neutron matter.
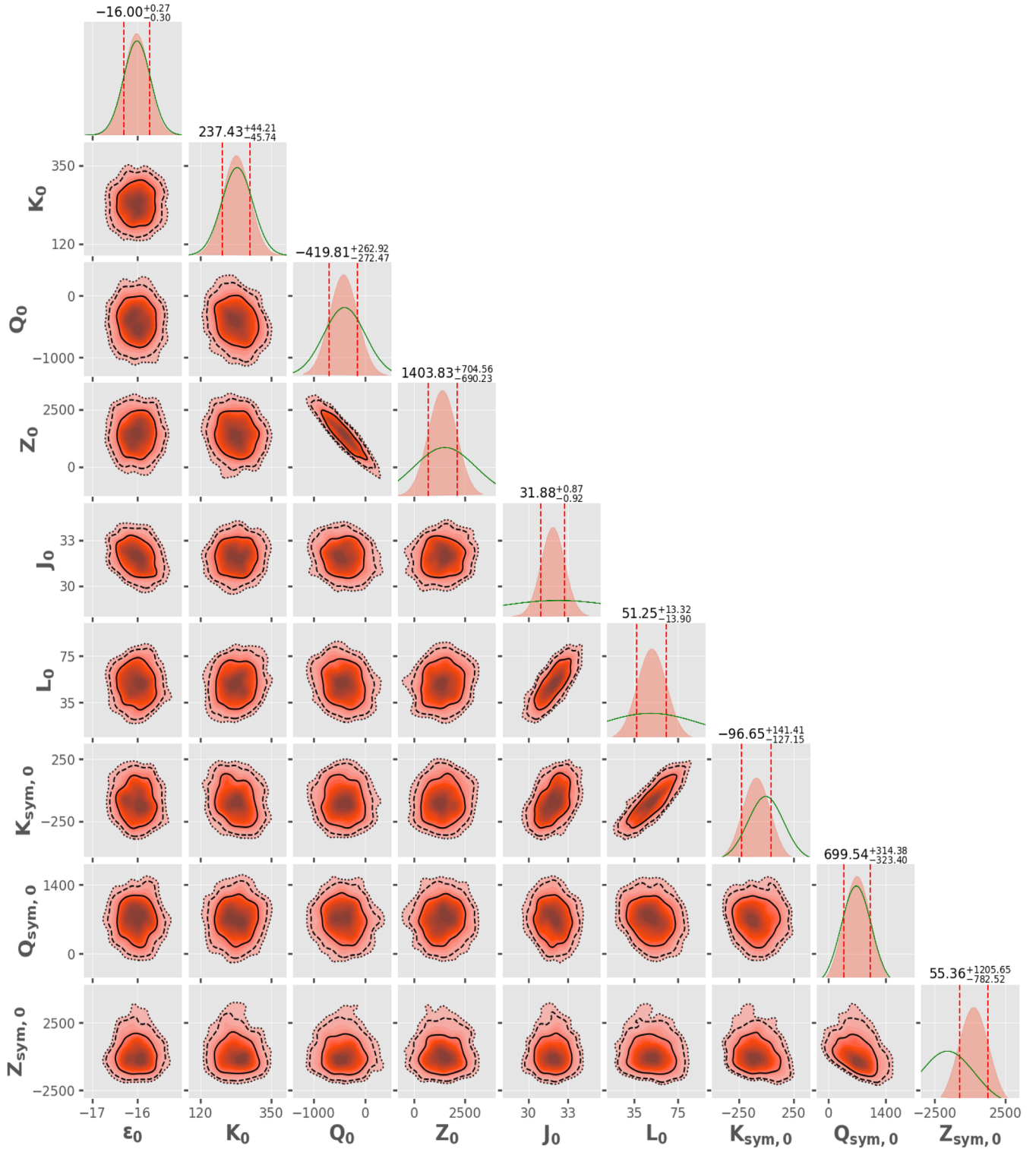
FIG. 1. Corner plots for the nuclear matter parameters (in MeV) obtained for Taylor expansions for the EOS of asymmetric nuclear matter. The one-dimensional marginalized posterior distributions (salmon) and the prior distributions (green lines) are displayed along the diagonal plots. The vertical lines indicate a 68% confidence interval of nuclear matter parameters. The confidence ellipses for two-dimensional posterior distributions are plotted with 1σ, 2σ, and 3σ confidence intervals along the off-diagonal plots. The distributions of nuclear matter parameters are obtained by subjecting them to minimal constraints (see the text for details).
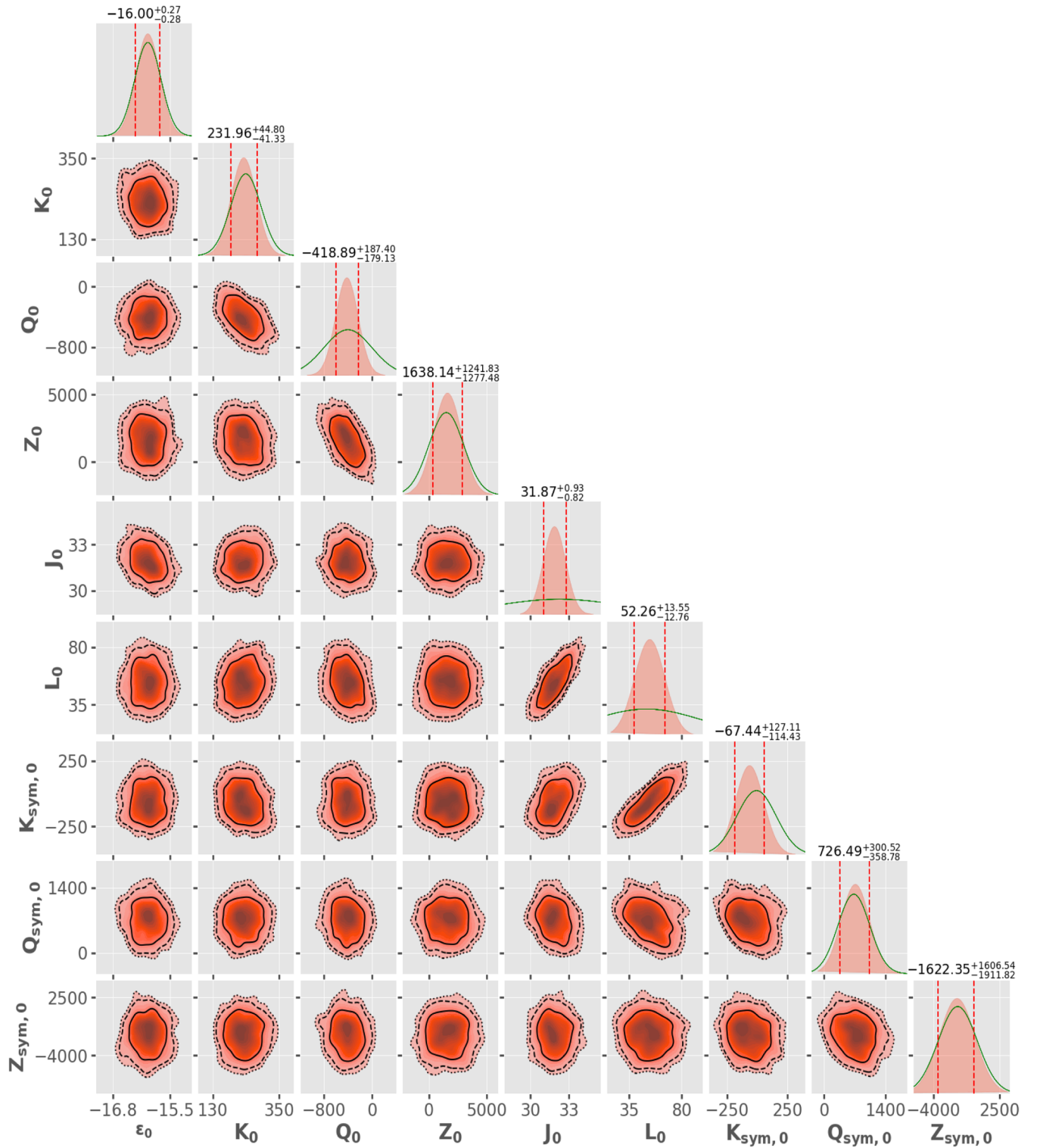
FIG. 2. The same as Fig. 1, but for $\frac{n}{3}$ expansions for the EOS of asymmetric nuclear matter.

The posterior distributions of $\Lambda_{1.4}$ and $R_{1.4}$ for both the expansions are quite close to each other. The differences begin to appear for the case of $R_{2.07}$, which become even larger for the maximum mass. This is due to the fact that the Taylor EOSs are much more stiffer than those for $\frac{n}{3}$.

The dichotomy in the high-density behavior of the Taylor and $\frac{n}{3}$ expansions would help us to understand the extent to which the correlations of the EOSs with the properties of NSs, for masses in the range $1-2\ M_\odot$, are model dependent. It is clear from off-diagonal plots that $\Lambda_{1.4}$ is strongly
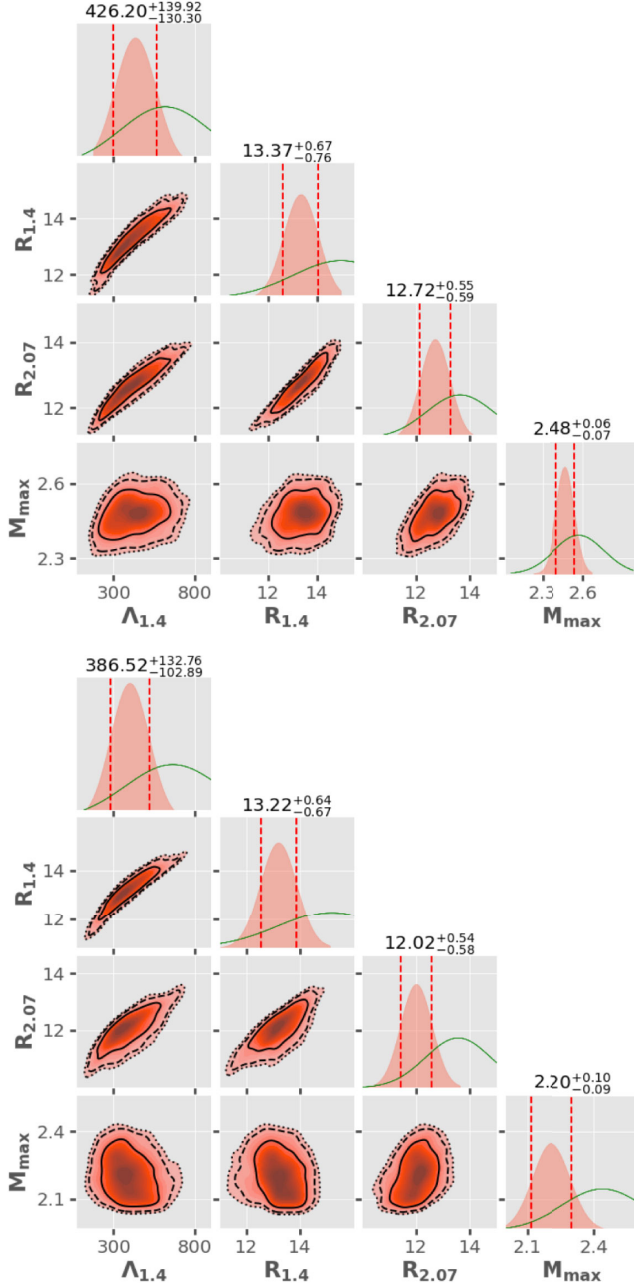
FIG. 3. Corner plots for the marginalized posterior distributions (salmon) of the tidal deformability $\Lambda_{1.4}$, radii $R_{1.4}$ (km) and $R_{2.07}$ (km), and the maximum mass M_{max} ($M_\odot$) for Taylor (top) and $\frac{n}{3}$ (bottom) expansions. The green lines represent effective priors obtained using the priors for nuclear matter parameters (see also Table I).

correlated with $R_{1.4}$, and the correlation coefficient is $r \sim 0.9$. The $\Lambda_{1.4}$ and $R_{1.4}$ also display stronger correlations with $R_{2.07}$ ($r \sim 0.8$) for the case of Taylor and somewhat moderate correlations ($r \sim 0.7$) for the $\frac{n}{3}$ expansion. The maximum mass of the neutron star is almost uncorrelated with the other NS properties considered.

We have summarized in Table IV (see the Appendix) the median values of NS properties along with 68% (90%)

confidence intervals. Like in the case of nuclear matter parameters, the NS properties get significantly constrained by the EOS of pure neutron matter at low density. For instance, the median values of $\Lambda_{1.4}$ become smaller by about 15% and the associated uncertainties by about 40% with the pure neutron matter constraints. The median values of $R_{1.4}$ and the corresponding uncertainties also become noticeably smaller. The $R_{2.07}$ and M_{max} do not show significant changes with the inclusion of low-density pure neutron matter constraints. With the PNM constraints, the 90% confidence interval of the neutron star properties such as tidal deformability, radius, and mass overlap with the currently available bounds $\Lambda_{1.4} \in [70, 580]$ [4], $R_{1.4} \in [11.41, 13.61]$ km [91], $R_{2.07} \in [11.8, 13.1]$ km [92], and $M_{max} \geq 2.09\, M_\odot$ [93]. The $M_{max} = 2.48^{+0.06}_{-0.07}\, M_\odot$ obtained for the Taylor EOSs is on the slightly higher side in comparison to the ones derived by combining the GW170817 observations of merging of binary neutron stars and quasiuniversal relation [94]. The observed electromagnetic emissions in the form of a kilonova and the detection of a gamma-ray burst have been linked to the formation of a black hole and, thus, have been utilized to infer the maximum mass of a stable neutron star. However, such inference of the maximum mass is subjected to uncertainties originating from model dependence of postmerger dynamics. Recent observation of the GW190814 event, a neutron star black hole–binary neutron star merger, has triggered an assessment of the maximum mass of a stable neutron star [95]. While there are different opinions available in the literature, the nature of a compact object in the range of 2.5–2.67 $M_\odot$ being a neutron star or black hole seems to be an unsettled issue to date [94–99]. So the maximum mass (M_{max}) we got for the Taylor model supporting the static NS of mass greater than 2.5 $M_\odot$ may not be ruled out at present.

We obtain joint probability distribution $P(M, R)$ for a given mass and radius for both the Taylor and $\frac{n}{3}$ expansions. They display qualitatively very much similar trends. In Fig. 4, we plot the $P(M, R)$ obtained for the $\frac{n}{3}$ expansion. The 90% confidence interval is represented by a red dashed line. The color gradient from orange to dark purple represents the lowest to highest probability. The most probable values for $R_{1.4}$ and $R_{2.07}$ are approximately 13.3 and 12.3 km, respectively. The $P(M, R)$ is maximum for $M \sim 1.4$–2.0 $M_\odot$ and $R \sim 12.4$–13.4 km. The 90% confidence interval has significant overlap with LIGO-Virgo and NICER estimations. It may be, however, pointed out that the main objective of the present work is to construct large sets of EOSs with diverse behavior to assess various correlation systematics as follows.

D. Correlations of neutron star properties with EOSs

We randomly select 1000 EOSs and corresponding NS properties from marginalized posterior distributions obtained for the Taylor as well as $\frac{n}{3}$ expansions. They
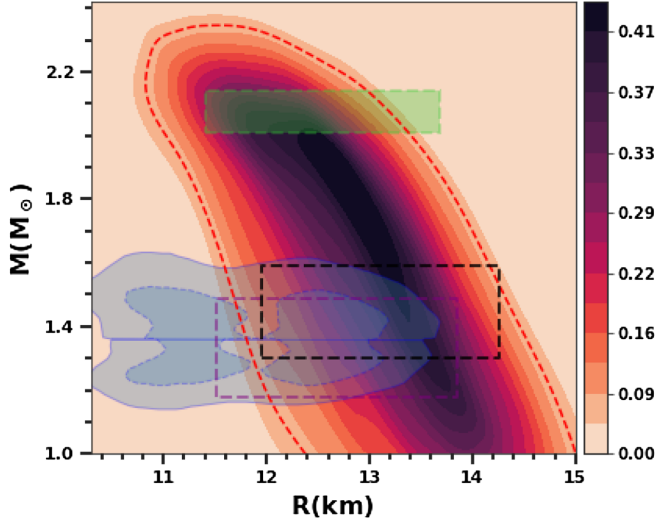
FIG. 4. Plot for joint probability distribution $P(M, R)$ as a function of the mass and radius of the neutron star obtained for $\frac{n}{3}$ expansion. The red dashed line represents the 90% confidence interval. The outer and inner gray shaded regions indicate the 90% (solid) and 50% (dashed) confidence interval of the LIGO-Virgo analysis for the BNS component from the GW170817 event [100–102]. The rectangular regions enclosed by dotted lines indicate the constraints from the millisecond pulsar PSR J0030 + 0451 (purple and black) NICER x-ray data [103,104] and PSR J0740 + 6620 (green) [92].

FIG. 5. The correlation coefficients $r(x, P_{BEM}(\rho))$, as approximated by both Taylor and $\frac{n}{3}$ expansion along with the mean-field theory calculations, are shown in this figure. Here, x represents either of the tidal deformability $\Lambda_{1.4}$, radii $R_{1.4}$ and $R_{2.07}$, or maximum mass M_{max} of the neutron star, whereas $P_{BEM}(\rho)$ represents the pressure for β-equilibrated matter at a density ρ. The calculations are performed with neutron star properties obtained using marginalized posterior distributions of nuclear matter parameters in Taylor and $\frac{n}{3}$ expansions. For comparison, the results are also displayed for a diverse set of nonrelativistic and relativistic microscopic MFMs.

are used to study the correlations of various NS properties with key quantities determining the behavior of the EOS. The correlations of $\Lambda_{1.4}$, $R_{1.4}$, $R_{2.07}$, and M_{max} with the pressure of β-equilibrated matter over a wide range of densities are evaluated. The values of correlation coefficients are plotted as a function of the density in Fig. 5. We also display the values of correlation coefficients for NS properties with the pressure of β-equilibrated matter calculated using unified EOSs for a diverse set of 41 non-relativistic and relativistic MFMs [89]. The various NS properties considered show strong correlations with $P_{BEM}(\rho)$ around a particular density. The density at which the correlation is maximum increases with the NS mass. The values of $\Lambda_{1.4}$ and $R_{1.4}$ are strongly correlated with $P_{BEM}(\rho)$ at density ~ 1.5–$2.5\rho_0$. The $R_{2.07}$ is strongly correlated with $P_{BEM}(\rho)$ around $3\rho_0$. The M_{max} is strongly correlated with $P_{BEM}(\rho)$ around $4.5\rho_0$. Our results for the Taylor and $\frac{n}{3}$ expansions for the region of maximum correlations are in line with those obtained using a diverse set of mean-field models, except for the case of $R_{2.07}$. Thus, it seems possible that the EOS over a range of densities beyond ρ_0 can be constrained in a nearly model-independent manner with the help of various NS observables.

In Table V (see the Appendix), we list the values of correlation coefficients obtained between the NS properties and the EOSs at some selected densities. The correlation
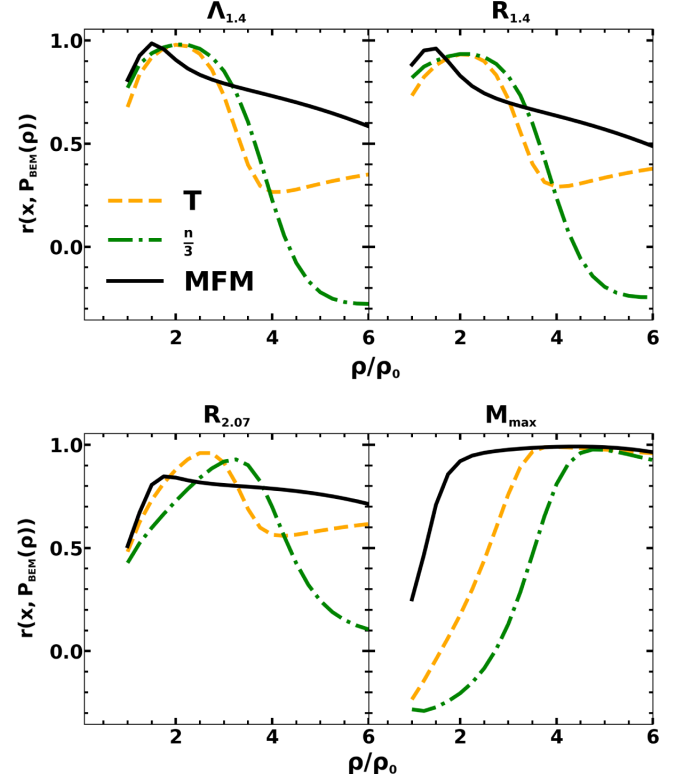
coefficients are obtained using 100 and 1000 EOSs, corresponding to Taylor and $\frac{n}{3}$ expansions, randomly selected from the posterior distributions. We also present the results which are obtained by combining 1000 EOSs corresponding to each of the expansions. The values of correlation coefficients for the combined set of EOSs are close to those obtained separately. The values of the correlation coefficients are close to those obtained for mean-field models listed in second column. We plot in Fig. 6 the variations of $P_{BEM}(\rho)$, at selected densities, with $\Lambda_{1.4}$, $R_{1.4}$, $R_{2.07}$, and M_{max} for which the correlations are stronger. We compare our results with those obtained from a diverse set of mean-field models. The correlation lines obtained by combining results of the Taylor and $\frac{n}{3}$ expansions are also plotted to estimate the values of $P_{BEM}(\rho)$ at selected densities with the help of NS properties. The equations for the correlation lines are obtained using linear regression as

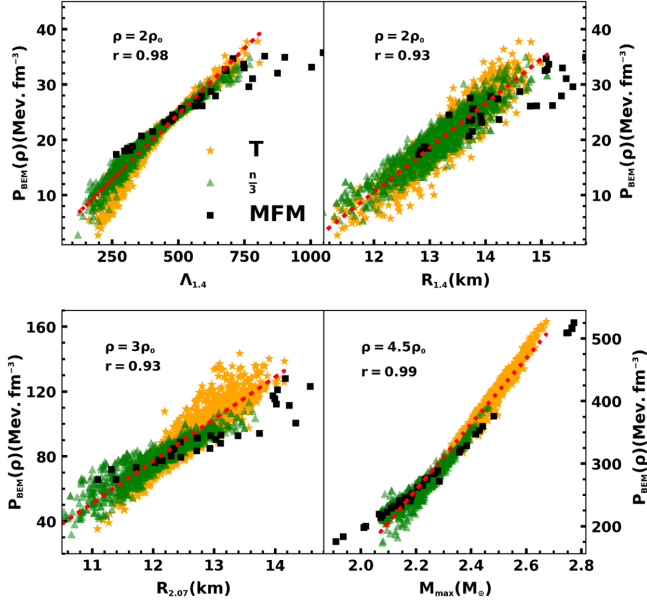FIG. 6. The variations of pressure for β-equilibrated matter $[P_{\mathrm{BEM}}(\rho)]$ at selected densities versus tidal deformability $\Lambda_{1.4}$, radii $R_{1.4}$ and $R_{2.07}$, and maximum mass M_{max} of the neutron star. The red dashed lines are obtained by linear regression [see Eq. (17) in Sec. III D].

$$\frac{P_{\mathrm{BEM}}(2\rho_0)}{\mathrm{MeV\,fm^{-3}}} = (0.96 \pm 0.10) + (0.0473 \pm 0.0002)\Lambda_{1.4},$$

$$\frac{P_{\mathrm{BEM}}(2\rho_0)}{\mathrm{MeV\,fm^{-3}}} = (-85.63 \pm 0.89) + (8.01 \pm 0.06)\frac{R_{1.4}}{\mathrm{km}},$$

$$\frac{P_{\mathrm{BEM}}(3\rho_0)}{\mathrm{MeV\,fm^{-3}}} = (-233.16 \pm 2.85) + (25.86 \pm 0.23)\frac{R_{2.07}}{\mathrm{km}},$$

$$\frac{P_{\mathrm{BEM}}(4.5\rho_0)}{\mathrm{MeV\,fm^{-3}}} = (-895.85 \pm 4.00) + (524.75 \pm 1.70)\frac{M_{\mathrm{max}}}{M_\odot}.$$

$$(17)$$

We extend our analysis for the correlations of the pressure for the β-equilibrated matter with tidal deformability over a wide range of neutron star mass. In Fig. 7, we display a color-coded graph for the correlations of tidal deformability of neutron stars for the mass 1.2–2.0 $M_\odot$ with the pressure for β-equilibrated matter at densities 0.5–5ρ_0 $[r(\Lambda_M, P_{\mathrm{BEM}}(\rho))]$. One can easily obtain the value of the correlation coefficient as a function of the density at a given NS mass. The $P_{\mathrm{BEM}}(\rho)$ at $\rho \sim 1.5$–2.5ρ_0 are strongly correlated ($r \sim 0.8$–1) with tidal deformability for NS masses in the range 1.2–2.0 $M_\odot$. Hence, $P_{\mathrm{BEM}}(\rho)$ can be parametrized at a given ρ as

$$\frac{P_{\mathrm{BEM}}(\rho)}{\mathrm{MeV\,fm^{-3}}} = a(M) + b(M)\Lambda_M, \qquad (18)$$

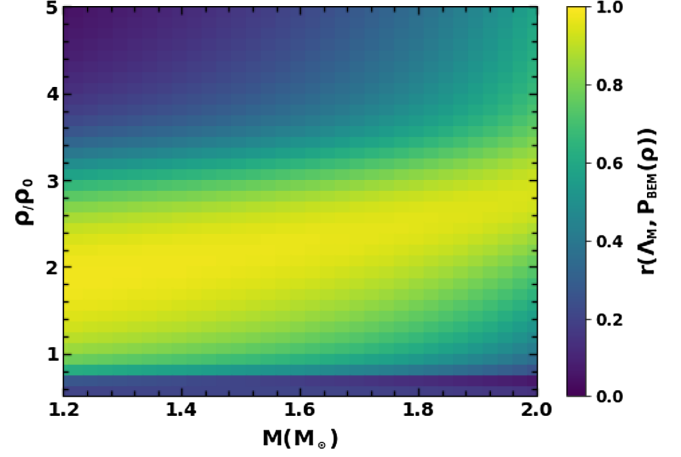with mass-dependent coefficients $a(M)$ and $b(M)$ expanded as

FIG. 7. Dependence of correlation coefficients between tidal deformability (Λ_M) and the pressure of β-equilibrated matter $[P_{\mathrm{BEM}}(\rho)]$ on neutron star mass (M) and density (ρ) is depicted in this plot. Here, $\rho_0 = 0.16$ fm^{-3} is used only for scaling purposes.

$$a(M) = (a_0 + a_1(M - M_0) + a_2(M - M_0)^2), \qquad (19)$$

$$b(M) = (b_0 + b_1(M - M_0) + b_2(M - M_0)^2), \qquad (20)$$

respectively, where M_0 is taken to be 1.4 $M_\odot$ and the values of a_i and b_i are estimated using a Bayesian approach with the help of $P_{\mathrm{BEM}}(\rho)$ and tidal deformability obtained for Taylor and $\frac{n}{3}$ expansions. For a given ρ, Eq. (18) is fitted using the tidal deformability corresponding to NS mass 1.2–2.0 $M_\odot$. The priors for a_i and b_i are taken to be uniform in the range of -100 to 100. The calculations are performed for $\rho = 1.5$, 2.0, and 2.5ρ_0. All the a_i's are strongly correlated with corresponding b_i's. The median values of parameters a_i and b_i and associated uncertainties are summarized in Table II. It may be noticed that the values of a_0 and b_0 for the case of $P_{\mathrm{BEM}}(2\rho_0)$ are not the same as those in Eq. (17). This may be partly due to the strong correlations between a_0 and b_0 of Eq. (18). Moreover, Eq. (17) is fitted to the values of tidal deformability at a fixed NS mass 1.4 $M_\odot$. To validate our parametrized form for $P_{\mathrm{BEM}}(\rho)$, we have calculated the values of $P_{\mathrm{BEM}}(2\rho_0)$ using Eq. (18) with the help of tidal deformability for 1.4 $M_\odot$ obtained for a large number of mean-field models which includes the one considered in Fig. 5 along with those taken from Refs. [23,81,105]. The average deviation of $P_{\mathrm{BEM}}(2\rho_0)$, obtained using Eq. (18), from the actual values is about 10%. We find marginal improvement when the terms corresponding to quadratic in tidal deformability are included in Eq. (18).

In Fig. 8, we display the variations of tidal deformability as a function of the mass and pressure for β-equilibrated matter at $\rho = 1.5$, 2.0, and 2.5ρ_0. These results are obtained

TABLE II. The median values and associated 68% (90%) uncertainties for the parameters, appearing in Eq. (18), obtained from their marginalized posterior distributions. The values of parameters b_0, b_1, and b_2 as listed are scaled up by a factor of 10.

Pressure (in MeV fm^{-3})	a_0	a_1	a_2	b_0	b_1	b_2
$P_{\mathrm{BEM}}(1.5\rho_0)$	$0.544^{+0.031(0.050)}_{-0.029(0.060)}$	$1.869^{+0.158(0.260)}_{-0.161(0.309)}$	$7.451^{+0.237(0.390)}_{-0.234(0.450)}$	$0.176^{+0.001(0.001)}_{-0.001(0.002)}$	$0.740^{+0.004(0.007)}_{-0.004(0.008)}$	$1.152^{+0.013(0.021)}_{-0.012(0.025)}$
$P_{\mathrm{BEM}}(2\rho_0)$	$0.146^{+0.030(0.050)}_{-0.030(0.059)}$	$-0.598^{+0.163(0.269)}_{-0.159(0.320)}$	$27.909^{+0.233(0.397)}_{-0.240(0.469)}$	$0.493^{+0.001(0.001)}_{-0.001(0.002)}$	$2.234^{+0.004(0.007)}_{-0.004(0.008)}$	$3.728^{+0.012(0.021)}_{-0.012(0.025)}$
$P_{\mathrm{BEM}}(2.5\rho_0)$	$7.345^{+0.030(0.050)}_{-0.030(0.060)}$	$-15.102^{+0.161(0.272)}_{-0.167(0.321)}$	$68.411^{+0.239(0.396)}_{-0.238(0.475)}$	$0.906^{+0.001(0.001)}_{-0.001(0.002)}$	$4.518^{+0.004(0.007)}_{-0.004(0.008)}$	$8.115^{+0.012(0.021)}_{-0.012(0.025)}$

using the parametrized form for $P_{\mathrm{BEM}}(\rho)$ as given by Eq. (18). One can easily estimate the values of $P_{\mathrm{BEM}}(\rho)$ for $\rho \sim 2\rho_0$ once the values of tidal deformability known in NS mass ranges 1.2–2.0 $M_\odot$.
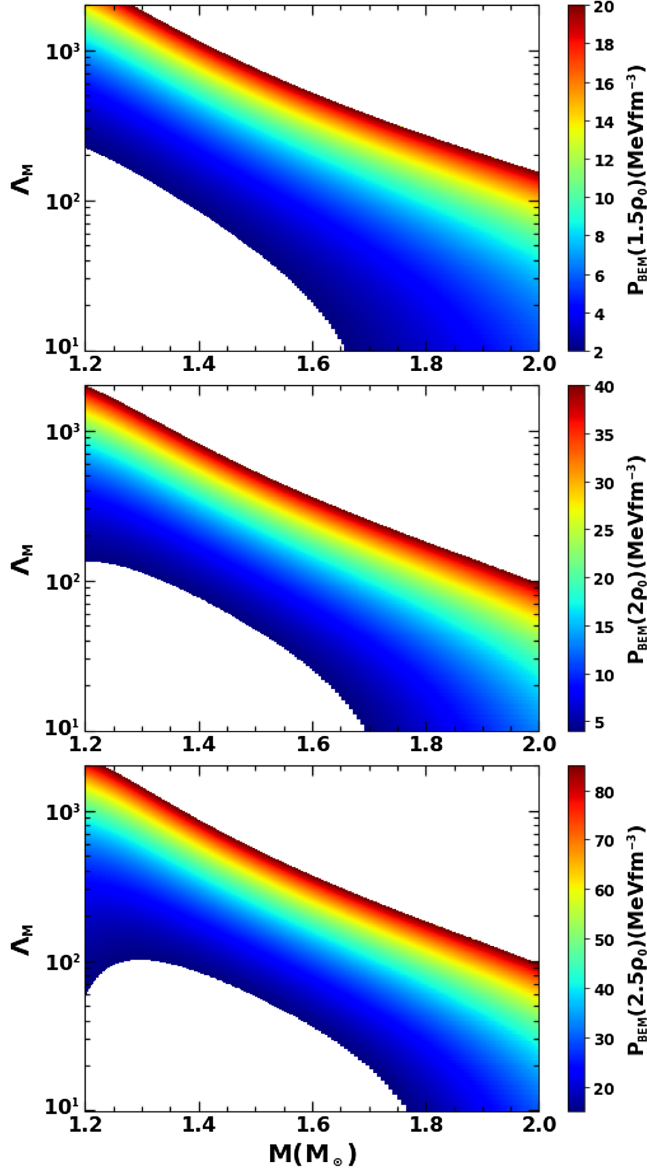

FIG. 8. The median values of pressure for β-equilibrated matter is shown here as a function of the neutron star mass and its tidal deformability at densities $1.5\rho_0$ (top), $2.0\rho_0$ (middle), and $2.5\rho_0$ (bottom).

IV. CONCLUSIONS

We have used Taylor and $\frac{n}{3}$ expansions of equations of state to construct marginalized posterior distributions of the nuclear matter parameters which are consistent with the minimal constraints. Only a few low-order nuclear matter parameters, such as the energy per nucleon, incompressibility coefficient for the symmetric nuclear matter, and symmetry energy coefficients at the saturation density (ρ_0), are constrained in narrow windows along with the low-density pure neutron matter EOS obtained from a precise N^{3}LO calculation in chiral effective field theory. The tidal deformability, radius, and maximum mass are evaluated using large sets of minimally constrained EOSs.

The correlations of neutron star properties over a wide range of mass with various key quantities characterizing the EOSs are investigated. We find that the values of tidal deformability and radius for the neutron star with 1.4 $M_\odot$ are strongly correlated with the pressure for the β-equilibrated matter at density $\sim 2\rho_0$. The radius for 2.07 $M_\odot$ neutron star is strongly correlated with the pressure for β-equilibrated matter at density $\sim 3\rho_0$. The maximum mass of the neutron star is correlated with the pressure for the β-equilibrated matter at density $\sim 4.5\rho_0$. These correlation systematics are in harmony with those obtained for unified EOSs for the β-equilibrated matter available for a diverse set of nonrelativistic and relativistic mean-field models. We exploit the model independence of correlations to parametrize the pressure for β-equilibrated matter, in the density range 1.5–2.5ρ_0, in terms of the mass and corresponding tidal deformability of the neutron star. Such a parametric form may facilitate a back-of-the-envelope estimation of the pressure at densities around 2ρ_0 for a given value of tidal deformability of neutron stars with mass in the range of 1.2–2.0 $M_\odot$.

APPENDIX: SOME USEFUL TABLES

We present our results in tabular form which are obtained with the minimal constraints. The values of the nuclear matters, properties of neutron stars, and their correlations with various key quantities associated with EOSs are listed in Tables III–V. These results are depicted in Figs. 1–6.

TABLE III. The median values and associated 68% (90%) uncertainties for the nuclear matter parameters from their marginalized posterior distributions. The results are obtained for Taylor and $\frac{n}{3}$ expansions with and without PNM constraints.

NMPs (in MeV)	Without PNM		With PNM	
	Taylor	$\frac{n}{3}$	Taylor	$\frac{n}{3}$
ε_0	$-16.02^{+0.23(0.41)}_{-0.28(0.56)}$	$-15.99^{+0.27(0.43)}_{-0.27(0.51)}$	$-16.00^{+0.27(0.42)}_{-0.30(0.54)}$	$-16.00^{+0.27(0.44)}_{-0.28(0.56)}$
K_0	$236.42^{+42.78(74.34)}_{-42.58(79.62)}$	$233.38^{+48.94(76.14)}_{-42.73(83.95)}$	$237.43^{+44.24(72.25)}_{-45.75(83.22)}$	$231.96^{+44.80(72.94)}_{-41.33(76.63)}$
Q_0	$-436.23^{+273.36(419.17)}_{-306.50(603.76)}$	$-411.84^{+207.53(301.56)}_{-210.88(409.00)}$	$-419.81^{+262.95(437.69)}_{-272.47(531.58)}$	$-418.89^{+187.43(300.76)}_{-179.25(377.42)}$
Z_0	$1441.51^{+792.45(1298.64)}_{-696.39(1381.30)}$	$1600.07^{+1067.33(1883.00)}_{-1362.28(2615.10)}$	$1403.84^{+704.56(1133.85)}_{-690.82(1386.25)}$	$1638.14^{+1241.83(1906.75)}_{-1277.48(2244.25)}$
J_0	$32.37^{+4.08(6.79)}_{-4.26(8.83)}$	$32.37^{+4.69(7.22)}_{-4.71(10.23)}$	$31.88^{+0.87(1.43)}_{-0.92(-1.85)}$	$31.87^{+0.93(1.49)}_{-0.82(1.68)}$
L_0	$59.88^{+41.14(65.90)}_{-39.84(78.17)}$	$55.60^{+37.59(63.89)}_{-43.88(84.62)}$	$51.25^{+13.32(21.60)}_{-13.91(25.54)}$	$52.25^{+13.55(22.73)}_{-12.76(23.04)}$
$K_{sym,0}$	$-85.86^{+192.67(327.83)}_{-151.57(266.76)}$	$-40.03^{+161.60(271.89)}_{-135.08(234.67)}$	$-96.65^{+141.41(225.69)}_{-127.49(216.74)}$	$-67.44^{+127.18(206.09)}_{-114.80(200.38)}$
$Q_{sym,0}$	$731.13^{+308.54(543.01)}_{-347.82(669.47)}$	$705.36^{+311.23(511.39)}_{-352.72(727.86)}$	$699.56^{+324.38(521.95)}_{-323.52(639.30)}$	$726.49^{+300.40(510.33)}_{-358.51(631.86)}$
$Z_{sym,0}$	$-2.07^{+1190.67(2153.84)}_{-820.92(1473.09)}$	$-1390.39^{+1518.69(2526.53)}_{-1856.18(3623.74)}$	$55.34^{+1205.62(2255.28)}_{-782.52(1415.84)}$	$-1622.35^{+1606.61(2788.70)}_{-1911.81(3468.40)}$

TABLE IV. Similar to Table III, but for the neutron star properties, namely, the tidal deformability ($\Lambda_{1.4}$), radii ($R_{1.4}$ and $R_{2.07}$), and maximum mass (M_{max}).

NS properties	Without PNM		With PNM	
	Taylor	$\frac{n}{3}$	Taylor	$\frac{n}{3}$
$\Lambda_{1.4}$	$527.72^{+250.72(477.68)}_{-186.11(292.57)}$	$455.85^{+223.65(465.72)}_{-163.05(243.23)}$	$426.20^{+139.93(224.58)}_{-130.32(205.18)}$	$386.52^{+132.76(213.24)}_{-102.84(199.09)}$
$R_{1.4}$ (km)	$14.69^{+1.78(3.43)}_{-1.63(2.74)}$	$14.15^{+1.87(3.34)}_{-1.69(2.58)}$	$13.37^{+0.67(1.03)}_{-0.75(1.60)}$	$13.22^{+0.64(0.99)}_{-0.67(1.59)}$
$R_{2.07}$ (km)	$13.24^{+0.82(1.49)}_{-0.82(1.42)}$	$12.27^{+0.88(1.52)}_{-0.80(1.52)}$	$12.72^{+0.55(0.85)}_{-0.59(1.07)}$	$12.02^{+0.54(0.88)}_{-0.58(1.23)}$
M_{max} ($M_\odot$)	$2.45^{+0.07(0.11)}_{-0.06(0.13)}$	$2.19^{+0.10(0.19)}_{-0.09(0.09)}$	$2.48^{+0.06(0.10)}_{-0.07(0.14)}$	$2.20^{+0.10(0.16)}_{-0.09(0.11)}$

TABLE V. The comparison of values for Pearson's correlation coefficient (r) obtained from randomly selected 100 and 1000 EOSs using both Taylor and $\frac{n}{3}$ expansions. The values of correlation coefficients are also obtained by combining 1000 EOSs from each of the expansions. For comparison, the values of r obtained for a diverse set of mean-field models are also presented in the second column.

	MFM	Taylor		$\frac{n}{3}$		Combined
Name of pairs	41	100	1000	100	1000	2000
$\Lambda_{1.4}$-$P_{BEM}(2\rho_0)$	0.90	0.98	0.98	0.99	0.98	0.98
$R_{1.4}$-$P_{BEM}(2\rho_0)$	0.83	0.93	0.93	0.94	0.93	0.93
$R_{2.07}$-$P_{BEM}(3\rho_0)$	0.81	0.93	0.91	0.92	0.92	0.93
M_{max}-$P_{BEM}(4.5\rho_0)$	0.99	0.97	0.98	0.95	0.96	0.99

[1] B. P. Abbott *et al.*, Phys. Rev. X **9**, 011001 (2019).
[2] B. P. Abbott *et al.*, Astrophys. J. **882**, L24 (2019).
[3] B. P. Abbott *et al.*, Astrophys. J. **892**, L3 (2020).
[4] B. P. Abbott *et al.*, Phys. Rev. Lett. **119**, 161101 (2017).
[5] T. Malik, N. Alam, M. Fortin, C. Providência, B. K. Agrawal, T. K. Jha, B. Kumar, and S. K. Patra, Phys. Rev. C **98**, 035804 (2018).
[6] S. De, D. Finstad, J. M. Lattimer, D. A. Brown, E. Berger, and C. M. Biwer, Phys. Rev. Lett. **121**, 091102 (2018).
[7] F. J. Fattoyev, J. Piekarewicz, and C. J. Horowitz, Phys. Rev. Lett. **120**, 172702 (2018).
[8] P. Landry and R. Essick, Phys. Rev. D **99**, 084049 (2019).
[9] J. Piekarewicz and F. J. Fattoyev, Phys. Rev. C **99**, 045802 (2019).
[10] T. Malik, B. K. Agrawal, J. N. De, S. K. Samaddar, C. Providência, C. Mondal, and T. K. Jha, Phys. Rev. C **99**, 052801 (2019).
[11] B. Biswas, P. Char, R. Nandi, and S. Bose, Phys. Rev. D **103**, 103015 (2021).
[12] H. D. Thi, C. Mondal, and F. Gulminelli, Universe **7**, 373 (2021).
[13] A. L. Watts *et al.*, Rev. Mod. Phys. **88**, 021001 (2016).
[14] M. C. Miller *et al.*, Astrophys. J. **887**, L24 (2019).
[15] T. Riley *et al.*, Astrophys. J. Lett. **887**, L21 (2019).
[16] N.-B. Zhang, B.-A. Li, and J. Xu, Astrophys. J. **859**, 90 (2018).
[17] B. J. Cai and B. A. Li, Phys. Rev. C **103**, 034607 (2021).
[18] H. Gil, P. Papakonstantinou, and C. H. Hyun, Int. J. Mod. Phys. E **31**, 2250013 (2022).
[19] J. M. Lattimer and M. Prakash, Astrophys. J. **550**, 426 (2001).
[20] A. Maselli, V. Cardoso, V. Ferrari, L. Gualtieri, and P. Pani, Phys. Rev. D **88**, 023007 (2013).
[21] B. P. Abbott *et al.*, Phys. Rev. Lett. **121**, 161101 (2018).
[22] Y. Lim and J. W. Holt, Phys. Rev. Lett. **121**, 062701 (2018).
[23] C. Y. Tsang, M. B. Tsang, P. Danielewicz, W. G. Lynch, and F. J. Fattoyev, Phys. Lett. B **796**, 1 (2019).
[24] C. Y. Tsang, M. B. Tsang, P. Danielewicz, W. G. Lynch, and F. J. Fattoyev, Phys. Rev. C **102**, 045808 (2020).
[25] G. Ashton *et al.*, Astrophys. J. Suppl. Ser. **241**, 27 (2019).
[26] S. Biscoveanu, E. Thrane, and S. Vitale, Astrophys. J. **893**, 38 (2020).
[27] M. W. Coughlin and T. Dietrich, Phys. Rev. D **100**, 043011 (2019).
[28] F. Hernandez Vivanco, R. Smith, E. Thrane, P. D. Lasky, C. Talbot, and V. Raymond, Phys. Rev. D **100**, 103009 (2019).
[29] S. Biscoveanu, S. Vitale, and C.-J. Haster, Astrophys. J. **884**, L32 (2019).
[30] M. E. Lower, E. Thrane, P. D. Lasky, and R. Smith, Phys. Rev. D **98**, 083028 (2018).
[31] I. M. Romero-Shaw, P. D. Lasky, and E. Thrane, Mon. Not. R. Astron. Soc. **490**, 5210 (2019).
[32] A. Ramos-Buades, S. Husa, G. Pratten, H. Estellés, C. García-Quirós, M. Mateu-Lucena, M. Colleoni, and R. Jaume, Phys. Rev. D **101**, 083015 (2020).
[33] I. M. Romero-Shaw, N. Farrow, S. Stevenson, E. Thrane, and X. J. Zhu, Mon. Not. R. Astron. Soc. **496**, L64 (2020).
[34] M. Zevin, C. P. L. Berry, S. Coughlin, K. Chatziioannou, and S. Vitale, Astrophys. J. **899**, L17 (2020).
[35] D. Keitel, Res. Notes AAS **3**, 46 (2019).
[36] G. Ashton and S. Khan, Phys. Rev. D **101**, 064037 (2020).
[37] E. Payne, C. Talbot, and E. Thrane, Phys. Rev. D **100**, 123017 (2019).
[38] Z. C. Zhao, H. N. Lin, and Z. Chang, Chin. Phys. C **43**, 075102 (2019).
[39] S. Wesolowski, N. Klco, R. J. Furnstahl, D. R. Phillips, and A. Thapaliya, J. Phys. G **43**, 074001 (2016).
[40] R. Somasundaram, C. Drischler, I. Tews, and J. Margueron, Phys. Rev. C **103**, 045803 (2021).
[41] C. Drischler, S. Han, J. M. Lattimer, M. Prakash, S. Reddy, and T. Zhao, Phys. Rev. C **103**, 045808 (2021).
[42] I. Tews, J. M. Lattimer, A. Ohnishi, and E. E. Kolomeitsev, Astrophys. J. **848**, 105 (2017).
[43] T. Carreau, F. Gulminelli, and J. Margueron, Phys. Rev. C **100**, 055803 (2019).
[44] H. D. Thi, T. Carreau, A. F. Fantina, and F. Gulminelli, Astron. Astrophys. **654**, A114 (2021).
[45] T. E. Riley, G. Raaijmakers, and A. L. Watts, Mon. Not. R. Astron. Soc. **478**, 1093 (2018).
[46] G. Raaijmakers *et al.*, Astrophys. J. Lett. **893**, L21 (2020).
[47] J.-L. Jiang, S.-P. Tang, Y.-Z. Wang, Y.-Z. Fan, and D.-M. Wei, Astrophys. J. **892**, 1 (2020).

[48] H. Güven, K. Bozkurt, E. Khan, and J. Margueron, Phys. Rev. C **102,** 015805 (2020).

[49] B. Biswas, Astrophys. J. **921,** 63 (2021).

[50] P. Landry, R. Essick, and K. Chatziioannou, Phys. Rev. D **101,** 123007 (2020).

[51] S. Huth et al., Nature (London) **606,** 276 (2022).

[52] B. Biswas, Astrophys. J. **926,** 75 (2022).

[53] S. M. A. Imam, N. K. Patra, C. Mondal, T. Malik, and B. K. Agrawal, Phys. Rev. C **105,** 015806 (2022).

[54] L.-W. Chen, C. M. Ko, and B.-A. Li, Phys. Rev. C **72,** 064309 (2005).

[55] L.-W. Chen, B.-J. Cai, C. M. Ko, B.-A. Li, C. Shen, and J. Xu, Phys. Rev. C **80,** 014322 (2009).

[56] W. G. Newton, J. Hooker, M. Gearheart, K. Murphy, D.-H. Wen, F. J. Fattoyev, and B.-A. Li, Eur. Phys. J. A **50,** 41 (2014).

[57] J. Margueron, R. Hoffmann Casali, and F. Gulminelli, Phys. Rev. C **97,** 025805 (2018).

[58] J. Margueron and F. Gulminelli, Phys. Rev. C **99,** 025806 (2019).

[59] J. M. Lattimer and M. Prakash, Phys. Rep. **621,** 127 (2016).

[60] H. Gil, P. Papakonstantinou, C. H. Hyun, T.-S. Park, and Y. Oh, Acta Phys. Pol. B **48,** 305 (2017).

[61] A. Gelman, J. B. Carlin, H. S. Stern, D. B. Dunson, A. Vehtari, D. B. Rubin, J. Carlin, H. Stern, D. Rubin, and D. Dunson, *Bayesian Data Analysis*, 3rd ed. (CRC Press, Boca Raton, FL, 2013).

[62] J. Buchner, A. Georgakakis, K. Nandra, L. Hsu, C. Rangel, M. Brightman, A. Merloni, M. Salvato, J. Donley, and D. Kocevski, Astron. Astrophys. **564,** A125 (2014).

[63] K. Hebeler, J. M. Lattimer, C. J. Pethick, and A. Schwenk, Astrophys. J. **773,** 11 (2013).

[64] E. Chabanat, P. Bonche, P. Haensel, J. Meyer, and R. Schaeffer, Nucl. Phys. **A635,** 231 (1998).

[65] E. Chabanat, P. Bonche, P. Haensel, J. Meyer, and R. Schaeffer, Nucl. Phys. **A627,** 710 (1997).

[66] C. Mondal, B. K. Agrawal, and J. N. De, Phys. Rev. C **92,** 024302 (2015).

[67] C. Mondal, B. K. Agrawal, J. N. De, and S. K. Samaddar, Phys. Rev. C **93,** 044328 (2016).

[68] A. Sulaksono, T. J. Buervenich, P. G. Reinhard, and J. A. Maruhn, Phys. Rev. C **79,** 044306 (2009).

[69] U. Garg and G. Colò, Prog. Part. Nucl. Phys. **101,** 55 (2018).

[70] B. K. Agrawal, S. Shlomo, and V. K. Au, Phys. Rev. C **72,** 014310 (2005).

[71] B. T. Reed, F. J. Fattoyev, C. J. Horowitz, and J. Piekarewicz, Phys. Rev. Lett. **126,** 172503 (2021).

[72] X. Roca-Maza, X. Viñas, M. Centelles, B. K. Agrawal, G. Colo', N. Paar, J. Piekarewicz, and D. Vretenar, Phys. Rev. C **92,** 064304 (2015).

[73] R. Essick, I. Tews, P. Landry, and A. Schwenk, Phys. Rev. Lett. **127,** 192701 (2021).

[74] M. Ferreira and C. Providência, Phys. Rev. D **104,** 063006 (2021).

[75] M. Dutra, O. Lourenco, J. S. Sa Martins, A. Delfino, J. R. Stone, and P. D. Stevenson, Phys. Rev. C **85,** 035201 (2012).

[76] M. Dutra, O. Lourenço, S. S. Avancini, B. V. Carlson, A. Delfino, D. P. Menezes, C. Providência, S. Typel, and J. R. Stone, Phys. Rev. C **90,** 055203 (2014).

[77] C. Mondal, B. K. Agrawal, J. N. De, S. K. Samaddar, M. Centelles, and X. Viñas, Phys. Rev. C **96,** 021302 (2017).

[78] C. Drischler, J. W. Holt, and C. Wellenhofer, Annu. Rev. Nucl. Part. Sci. **71,** 403 (2021).

[79] A. Ekström, G. R. Jansen, K. A. Wendt, G. Hagen, T. Papenbrock, B. D. Carlsson, C. Forssén, M. Hjorth-Jensen, P. Navrátil, and W. Nazarewicz, Phys. Rev. C **91,** 051301 (2015).

[80] Y. Lim and J. W. Holt, Eur. Phys. J. A **55,** 209 (2019).

[81] T. Malik, M. Ferreira, B. K. Agrawal, and C. Providência, Astrophys. J. **930,** 17 (2022).

[82] S. Ghosh, B. K. Pradhan, and D. Chatterjee, and J. Schaffner-Bielich, Front. Astron. Space Sci. **9,** 864294 (2022).

[83] N. K. Glendenning, Phys. Rev. D **46,** 4161 (1992).

[84] D. Adhikari et al. (PREX Collaboration), Phys. Rev. Lett. **126,** 172502 (2021).

[85] J. R. Oppenheimer and G. M. Volkoff, Phys. Rev. **55,** 374 (1939).

[86] R. C. Tolman, Phys. Rev. **55,** 364 (1939).

[87] G. Baym, C. Pethick, and P. Sutherland, Astrophys. J. **170,** 299 (1971).

[88] J. Carriere, C. J. Horowitz, and J. Piekarewicz, Astrophys. J. **593,** 463 (2003).

[89] M. Fortin, C. Providencia, A. R. Raduta, F. Gulminelli, J. L. Zdunik, P. Haensel, and M. Bejger, Phys. Rev. C **94,** 035804 (2016).

[90] J. Piekarewicz and F. J. Fattoyev, Phys. Rev. C **99,** 045802 (2019).

[91] M. C. Miller et al., Astrophys. J. Lett. **918,** L28 (2021).

[92] T. E. Riley et al., Astrophys. J. Lett. **918,** L27 (2021).

[93] R. W. Romani, D. Kandel, A. V. Filippenko, T. G. Brink, and W. Zheng, Astrophys. J. Lett. **908,** L46 (2021).

[94] L. Rezzolla, E. R. Most, and L. R. Weih, Astrophys. J. Lett. **852,** L25 (2018).

[95] R. Abbott et al. (LIGO Scientific, Virgo Collaborations), Astrophys. J. Lett. **896,** L44 (2020).

[96] A. Tsokaros, M. Ruiz, and S. L. Shapiro, Astrophys. J. **905,** 48 (2020).

[97] Y. Lim, A. Bhattacharya, J. W. Holt, and D. Pati, Phys. Rev. C **104,** L032802 (2021).

[98] C. Drischler, S. Han, J. M. Lattimer, M. Prakash, S. Reddy, and T. Zhao, Phys. Rev. C **103,** 045808 (2021).

[99] A. Li, Z. Miao, S. Han, and B. Zhang, Astrophys. J. **913,** 27 (2021).

[100] B. P. Abbott et al., Phys. Rev. Lett. **121,** 161101 (2018).

[101] B. P. Abbott et al., Phys. Rev. X **9,** 011001 (2019).

[102] R. Abbott et al., SoftwareX **13,** 100658 (2021).

[103] T. E. Riley et al., Astrophys. J. Lett. **887,** L21 (2019).

[104] M. C. Miller et al., Astrophys. J. Lett. **887,** L24 (2019).

[105] M. Ferreira, M. Fortin, T. Malik, B. K. Agrawal, and C. Providência, Phys. Rev. D **101,** 043021 (2020).

[106] I. M. Romero-Shaw et al., Mon. Not. R. Astron. Soc. **499,** 3295 (2020).